Published in final edited form as:
J Comp Neurol. 2012 May 1; 520(7): 1493–1508. doi:10.1002/cne.22807.

Tonotopic Organization of the Superior Olivary Nucleus in the Chicken Auditory Brainstem

Kathryn M. Tabor[1], **William L. Coleman**[2], **Edwin W Rubel**[1,3], and **R. Michael Burger**[2,*]

[1]Virginia Merrill Bloedel Hearing Research Center, Department of Otolaryngology, Head and Neck Surgery and Neurobiology and Behavior Graduate Program, University of Washington, Seattle, Washington 98195

[2]Department of Biological Sciences, Lehigh University, Bethlehem, Pennsylvania 18015

[3]Department of Physiology and Biophysics, University of Washington, Seattle, Washington 98195

Abstract

Topographic maps are salient features of neuronal organization in sensory systems. Inhibitory components of neuronal circuitry are often embedded within this organization, making them difficult to isolate experimentally. The auditory system provides opportunities to study the topographic organization of inhibitory long-range projection nuclei, such as the superior olivary nucleus (SON). We analyzed the topographic organization of response features of neurons in the SON of chickens. Quantitative methods were developed to assess and communicate this organization. These analyses led to three main conclusions: 1) sound frequency is linearly arranged from dorsal (low frequencies) to ventral (high frequencies) in SON; 2) this tonotopic organization is less precise than the organization of the excitatory nuclei in the chicken auditory brainstem; and 3) neurons with different response patterns to pure tone stimuli are interspersed throughout the SON and show similar tonotopic organizations. This work provides a predictive model to determine the optimal stimulus frequency for a neuron from its spatial location in the SON.

Indexing Terms

auditory; inhibitory; superior olivary nucleus; three-dimensional tonotopic organization

Topographic organization is a robust and salient feature of sensory and motor areas in the vertebrate brain. Anatomic and physiologic topography is thought to provide a neuronal substrate critical for processing sensory information. For example, location of a visual stimulus is encoded at the retina and then represented in “retinotopically” organized structures throughout the visual pathways. Similarly, in the auditory system, sound

*Correspondence to: R. Michael Burger, Ph. D., Dept. of Biological Sciences, Lehigh University, 111 Research Dr., Bethlehem, PA 18015. burger@lehigh.edu.
William L. Coleman's current address is Department of Biological and Allied Health Sciences, Bloomsburg University of Pennsylvania, Bloomsburg, PA, 17815.

Additional Supporting Material may be found in the online version of this article.

frequency encoded along the sensory epithelium gives rise to "tonotopic" maps throughout the central auditory pathways. Descriptions of maps provide information to understand how an external stimulus is represented and processed in the nervous system. Moreover, quantitative maps provide predictive tools to determine the optimal stimulus for a particular neuron based on its location in the tissue. Using this information investigators can 1) relate anatomical, biophysical, and pharmacological characteristics of a neuron to sensory processing based on stimulus selectivity (Smith and Rubel, 1979; Kuba et al., 2005); and 2) compare the precision of processing across sensory areas or across species.

Inhibitory components of many neuronal circuits comprise interneurons residing alongside principal neurons (Huang et al., 2007). Thus, independent evaluation of the organizing features of these circuit components is difficult. However, in the auditory brainstem, inhibitory neurons often reside in nuclei that project to one or more targets, thus providing opportunities to study sensory mapping in inhibitory long-range projection nuclei (Tsuchitani and Boudreau, 1966; Sanes and Friauf, 2000; Kim and Kandler, 2003). In the current study we use a quantitative strategy to describe the 3D tonotopic organization of the superior olivary nucleus (SON) in chicken. The avian SON comprises inhibitory neurons that provide long-range γ-aminobutyric acid (GABA)ergic and possibly glycinergic inhibition to other auditory nuclei in the brainstem (Yang et al., 1999; Kuo et al., 2009; Coleman et al., 2011). Inhibition from the SON expands the dynamic range and sharpens temporal coding of auditory neurons to enable sound localization (Burger et al., 2005; Nishino and Ohmori, 2009; Fukui et al., 2010).

The goal of the current study is to analyze the topographic organization of 1) sound frequency and 2) physiologically identified cell types. Specifically, is the tonotopic organization of the brainstem auditory pathway preserved in the SON? Past studies in the owl (Moiseff and Konishi, 1983) and chicken (Lachica et al., 1994; Tabor et al., 2011) have suggested that stimulus frequency may be systematically represented in the SON. Furthermore, the SON contains a heterogeneous mixture of response patterns to tone stimulation (Moiseff and Konishi, 1983; Tabor et al., 2011; Coleman et al., 2011). However, a detailed topographic map of these response features remains to be determined.

In addition to the physiological heterogeneity in SON, anatomical evidence suggests that the SON contains functionally distinct classes of neurons. Anatomically, multiple auditory pathways converge in the SON. One major input arises from the binaural coincidence detecting neurons in the nucleus laminaris (NL), whereas another arises from the ipsilateral nucleus angularis (NA) (Moiseff and Konishi, 1981, 1983; Takahashi et al., 1984). Also, distinct populations of SON neurons give rise to two projections, one to ipsilateral targets and the other to the contralateral SON and higher order centers (Conlee and Parks, 1986; Westerberg and Schwartz, 1995; Burger et al., 2005). Whether the physiologically distinct cell types correspond to the apparent functional classes of SON neurons revealed by anatomical projections remains unknown. Because SON neurons provide the majority of inhibition to all auditory nuclei in the dorsal brainstem (Lachica et al., 1994; Yang et al., 1999; Burger et al., 2005), it is important to understand how auditory information is processed in the SON.

By using in vivo single- and multiple-unit recordings we classified the characteristic frequency (CF), frequency selectivity, threshold, and response patterns of SON neurons. 3D reconstructions and quantitative analyses determined that CF is linearly mapped in the SON. This tonotopic organization is less precise than that of other auditory nuclei in the avian brainstem (Rubel and Parks, 1975). In addition, we found that SON neurons with onset and sustained response patterns are interspersed throughout the entire structure of the SON, and that both types show similar tonotopic organizations. These results suggest that both phasic and tonic SON responses are generated for all sound frequencies processed in the chicken auditory system. The quantitative 3D tonotopic map of the SON provides a powerful tool for future studies of neuronal circuitry in this system. These analytical methods will be broadly applicable to other sensory and motor system circuitry.

Materials and Methods

Experiments were conducted on white leghorn chicken hatchlings (*Gallus gallus domesticus*) 7–15 days old. All procedures were carried out in accordance with the National Institutes of Health Guide for the Care and Use of Laboratory Animals and approved by the Lehigh University Institutional Animal Care and Use Committee. All efforts were made to minimize pain and discomfort of the animals used and to minimize the animal number. Detailed experimental methods were reported previously (Coleman et al., 2011).

Surgery

Chickens (54–157 g) were anesthetized with an intramuscular injection of ketamine (80 mg/kg; Ketaset, Fort Dodge Animal Health, Fort Dodge, IA), an intraperitoneal injection of pentobarbital (80 mg/kg; Sigma-Aldrich, St. Louis, MO), and an intramuscular injection of urethane (4, 0.625 g/kg doses separated by 20–30 minutes; Sigma-Aldrich). Additional urethane (0.625 g/kg) was injected in some cases to maintain the level of anesthesia. The bird's body temperature was maintained at 40°C throughout all procedures by using a heating pad. A tracheotomy was performed to facilitate breathing during the experiment. The head was fixed to a stereotaxic stage and a brass rod was fastened to the top of the cranium with dental cement. After the cement cured, the animal was transferred to a customized stereotaxic apparatus inside a sound attenuation booth. The skin covering the skull was removed, and the skull was opened to expose the cerebellum. A slit was made in the dura mater for electrode penetration. Care was taken not to injure the large venous sinus.

Sound presentation and data acquisition

Freely available software (Spike; Brandon Warren, University of Washington) controlled acoustic stimuli generation and data acquisition. Sound stimuli were output through an HB7 Headphone Driver (Tucker-Davis Technologies, Alachua, FL) to an Eartone 3A Insert earphone coupled to the ipsilateral ear with a tube insulated with acoustic foam (Etymotic Research, Elk Grove Village, IL). The sound pressure level (SPL) was calibrated using a ¼” free-field microphone (model 2520; Larson-Davis, Provo, UT) and microphone preamp (model 221; Larson-Davis). The maximum sound intensity was 90 dB SPL, and the sound frequency range was 50–6,000 Hz. Tone duration was 20 or 40 ms with a 5-ms rise and fall time for a triangle-shaped envelope.

In vivo recording

Tungsten recording electrodes (5–8 MΩ; no. 575300, AM Systems, Sequim WA) were inserted 2.1–2.3 mm lateral and 0.0–0.5 mm rostral to the venous sinus. SON neuronal units were located by presenting a white-noise stimulus (65–70 dB SPL, 50-ms duration, 3 pulses/s) to the ipsilateral ear while advancing the electrode using a remotely driven actuator (MC1000e-1 Controller; Siskiyou Design Instruments, Grants Pass, OR). Neuronal action potentials were bandpass-filtered between 300 Hz and 3 kHz (model 3362 filter; Krohn-Hite, Brockton, MA) and amplified with a Neuroprobe Amplifier Model 1600 (A-M Systems, Carlsborg, WA). Both analog voltage traces and action potential event times were simultaneously recorded. Analog traces were collected with 12-bit resolution at 50-kHz sampling frequency. Action potential event times were recorded by using a voltage window discriminator (model 121; World Precision Instruments, Sarasota, FL). Both signals were processed by an RX6 Multifunction Processor (Tucker-Davis Technologies).

After isolation of a neuronal unit or cluster from background noise, the frequency tuning of the neuronal response was coarsely mapped to determine whether the unit responded to low-, middle-, or high-frequency acoustic stimuli. A high-resolution frequency response function was derived by presenting a series of low (0.05–2 kHz), middle (1–4 kHz), or high (2–5 or 6 kHz) tone stimuli (12 logarithmic steps, 20- or 40-ms duration, 10 pulses/s) at levels ranging from 0 to 90 dB SPL (10-dB steps). If responses from a neuronal unit spanned two frequency ranges, both stimulus sets were presented. Each stimulus was presented 20 times in a pseudo-randomized sequence. After recordings, small electrolytic lesions (~100 μm in diameter, 15 μA, 20 seconds to 1 minute) were made to mark the position of the electrode penetrations (see Fig. 4B) and to facilitate 3D reconstruction of SON.

Analysis of electrophysiological data

Single- and multiple-unit activity were sorted by using a freely available PostHawk program (David Schneider, Woolley Lab, Columbia University, New York, NY) written in MatLab (Mathworks, Natick, MA). Spike counts were obtained from a time window equal to the duration of the stimulus and adjusted to the minimum first latency of the response. For multiple-unit recordings, neuronal events were counted when the voltage trace exceeded two-thirds the peak voltage of the recording. We used event counts to calculate the rates of multiple-unit activity. Response threshold was defined as the intensity at which the spike rate (or rate of multiple-unit activity) during the stimulus time exceeded the average spontaneous rate by two SDs. Characteristic frequency (CF) was defined as the frequency with the lowest response threshold. Response patterns of neurons were classified from post-stimulus time histograms to tones of CF presented 20 dB above response threshold (Fig. 1). Frequency tuning curves were assessed by analyzing Q10, defined as the CF divided by the response bandwidth 10 dB above threshold.

Nissl staining

Following electrophysiological recording, animals were transcardially perfused with phosphate-buffered saline (PBS; 0.1 M, 7.2–7.4 pH) followed by chilled 4% paraformaldehyde in PBS. The brains were removed from the skull and postfixed overnight in the paraformaldehyde solution. Each brain was cut coronally at 40 μm on a freezing stage

of a sledge microtome, and each section was collected in PBS. Sections were maintained in order and stained for Nissl with thionin.

Imaging and 3D reconstruction

Brightfield images were captured by using a Zeiss Axioplan 2ie microscope (Carl Zeiss Microimaging, Thornwood, NY) equipped with a 4× (NA 0.09) objective and a CoolSnap HQ monochrome digital camera (Princeton Instruments, Trenton, NJ) and collected in Slidebook (version 4.0.2.8; Intelligent Imaging Innovations, Denver, CO). Selected images were further processed in Adobe Photoshop (Adobe Systems, Mountain View, CA) to enhance contrast and alter brightness for inclusion in figure illustrations. Images of all brainstem sections containing the right SON were aligned to form a z-stack using freely available stackreg plugin (Thevenaz et al., 1998) for ImageJ software (W.S. Rasband; NIH, Bethesda, MD). SONs were reconstructed in 3D from the aligned image stack by using Amira software (Visage Imaging, Berlin, Germany).

For each case, coordinates of electrolytic lesions and electrode tracks in the aligned image stack were compared with stereotaxic coordinates taken at the brain surface for each electrode penetration in order to map recording sites in the reconstructed SON (see Fig. 4). Multilinear regression analysis (MRA) with linear and log equations was used to examine the tonotopic organization of each case (Table 1).

For each SON reconstruction, we determined the ratio of lengths of the medial-lateral to dorsal-ventral to anterior-posterior axes (mean ± SD, 0.70 ± 0.07 to 0.59 ± 0.05 to 1). Also, we determined the orientation of the major axis of each SON reconstruction. For all cases, the anterior ends of the major axes pointed 17 ± 10° medial and 9 ± 6° ventral to the anterior-posterior axis.

We created a standardized SON containing all recording sites of 19 reconstructed SONs by using three steps. First, we translated the reconstructed SONs to overlay their centroids. Second, we rotated the reconstructed SONs to align their major axes to the mean orientation of the population (see above). Third, we normalized the lengths of the medial-lateral, dorsal-ventral, and anterior-posterior axes of all reconstructed SONs. All analyses of the combined dataset containing all recording sites used these normalized anatomical coordinates ranging from 0 to 1 along each axis. However, to visualize the standardized SON and its topographic organization, the lengths of the medial-lateral, dorsal-ventral, and anterior-posterior axes were scaled by the mean ratio of the population (0.7 to 0.59 to 1; see above) to preserve the anatomical shape of SON.

Principle component analysis (PCA) and MRA were used to determine the major tonotopic axis across the standardized SON. Three key steps were used to apply PCA to our experimental dataset. First, we organized the combined dataset into a 4×659 matrix. Each of the four rows contained one measurement type (medial-lateral coordinate, dorsal-ventral coordinate, anterior-posterior coordinate, CF) and each column contained data from one recording location. Second, we subtracted the mean and normalized the range of each measurement type, or row of the matrix. Third, we computed the eigenvectors and eigenvalues of the covariance matrix to determine the principal components. The orientation

of the first principal component was visualized in three spatial dimensions by using the first three values of the eigenvector associated with the medial-lateral, dorsal-ventral, and anteior-posterior dimensions, respectively.

MRA was performed on the combined dataset by using linear and log equations. The data were best fit by the multilinear regression function:

$$\mathrm{CF}=0.01+0.32/+4.09v-0.55a \quad (1)$$

where CF is the characteristic frequency in kHz, / is the normalized medial-lateral coordinate (lateral edge is 1), *v* is the normalized dorsal-ventral coordinate axis (ventral edge is 1), and *a* is the normalized anterior-posterior coordinate (anterior edge is 1).

To visualize the tonotopic dimensions (see Figs. 5, 6, and 8), we show the orientations of the first principal component and the multilinear regression equation with arrows passing through the “center of mass” of the recording sites. The center of mass of recording sites was defined as the mean of their positions in 3D.

For isolated neuronal responses, the spatial distributions of two physiological types of neurons (sustained and onset) were visualized and analyzed in the standardized SON. The tonotopic organization of each type was examined by using MRA (Table 1).

Statistical evaluations were made by using Student's t-test or r^2 correlation, and statistical significance was achieved when $P < 0.05$. All data are presented as mean ± SD.

Results

The results are presented in three main sections. First, we characterize several properties of SON neurons important for auditory processing: response patterns, frequency tuning and selectivity, and response threshold. Second, the 3D spatial organization of frequency tuning is reconstructed for each individual SON. Finally, these representations are projected onto a 3D standardized SON to provide a predictive tonotopic map and examine the spatial distribution of two neuronal response patterns in the SON.

Response patterns, frequency tuning and selectivity, and response threshold

By using in vivo recordings, we characterized the response properties of neurons in the SON to ipsilateral tones. Response patterns, CFs, widths of tuning curves, and response thresholds varied widely between SON neurons.

Figure 1 illustrates the response patterns of isolated single SON neurons to ipsilateral tones of CF presented at 20 dB above response threshold. Seventy-three percent of isolated neurons generated sustained responses, either primary-like (Fig. 1A) or pauser-like patterns (Fig. 1B), 25% of isolated neurons produced onset response patterns (Fig. 1C), and 2% suppressed activity in response to ipsilateral tones (Fig. 1D). These activity patterns, and the relative proportion of each response type are consistent with our previous characterization of the SON in chickens (Coleman et al., 2011). Complexity and diversity of SON neuronal

responses may derive from their multiple inputs. SON responses resemble the varied response types observed in NA neurons (Sachs et al., 1978; Carr and Soares, 2002; Koppl and Carr, 2003). Additionally, sustained responses in SON may also be evoked by sustained NL neuron inputs, which are weakly driven by monaural stimulation (Pena et al., 1996).

To examine frequency tuning of SON neurons, we constructed their frequency-level response maps. The patterns of excitatory and suppressed response regions of tuning curve plots differed widely between neurons. Representative tuning profiles are shown in Figure 2. Figure 2A shows a response map of an isolated neuron with a V-shaped excitatory region (gray lines) and suppressed responses to neighboring frequencies (red line). Figure 2B shows tones at CF driving excitatory responses of a neuron at intensities above response threshold, but suppressing responses of this neuron at lower sound levels. Figure 2C illustrates an example of a suppressed responder, which reduced its spike rate to a range of frequencies but showed no excitatory response areas.

To compare tuning and selectivity of these neurons, we measured their CF, Q10s, and response thresholds. Figure 3 shows the distributions of response properties of SON neurons to ipsilateral tones. Among the 310 multiple-units and 349 isolated neurons recorded in the SON, CF ranged from 90 to 5,000 Hz (Fig. 3A; see Fig. 3 legend for statistics). CF distributions of isolated neurons with sustained or onset response patterns represented the entire frequency range of hearing in chicken (Fig. 3B; Gray and Rubel, 1985; Saunders and Salvi, 1993). Next we measured the response thresholds at CF in the SON. Thresholds of multiple-unit responses tended to be slightly higher than the thresholds of isolated neuronal responses ($P < 0.01$; Fig. 3C). This increase reflects multiple-unit recordings with neuronal waveforms that individually were not detected by using our threshold criterion, but summed to form detectable waveforms at higher sound intensities. For isolated neurons, thresholds of both sustained and onset responders increased with CF (Fig. 3C,D). For example, average thresholds of sustained responders increased ~20 dB between CF of 100 and 5,000 Hz (Fig. 3D, bottom). Caution should be used when comparing thresholds between sustained and onset responders because the spike rate criterion used to determine response threshold (see Materials and Methods) may not be equally sensitive between categories of responders.

Finally, we assessed frequency selectivity of SON neurons by measuring Q10, which increases with selectivity and CF ($r^2 = 0.50$, $P < 0.01$). Sustained responders showed higher frequency selectivity, i.e., narrower tuning curves, than onset responders ($P < 0.01$; Fig. 3E). In summary, Figure 3 shows that CF, threshold, and Q10 distributions in the SON resemble other auditory brainstem nuclei in this species (Sachs et al., 1978; Warchol and Dallos, 1990).

3D reconstructions of SON and recording sites

Figure 4 illustrates how individual SONs and recording sites were reconstructed in 3D. Figure 4A shows coronal sections through the SON stained for Nissl. Consecutive sections containing the SON were aligned as described in Materials and Methods. By using the coordinates of the electrolytic lesions, approximately 100 μm in diameter (Fig. 4B, double arrowheads), and the positions of the electrode tracks (Fig. 4A,B, arrows), the recording sites were mapped onto the reconstructed SON for each case (see Materials and Methods).

The 3D reconstruction of the SON and locations of recordings are presented in the coronal (Fig. 4C) sagittal (Fig. 4D), and horizontal views (Fig. 4E). Supplemental Movie 1 shows a rotation of this 3D reconstruction (Fig. 4), to visualize the shape of SON and locations of recordings. Table 1 lists the number of recording sites and general region of the SON sampled in each case. We recorded from 12 to 75 sites per animal, and across all cases neuronal responses from all regions of SON were sampled. Because we were able to map recordings to precise locations in 3D SON reconstructions, these datasets could be used to quantitatively analyze the topographic organization of the SON.

Individual SON are tonotopically organized

By using 3D reconstructions of recording sites in the SON, we performed MRA to determine the tonotopic organization of individual SON in each animal. In the majority of cases, recording sites were clearly arranged from low CF located dorsally to high CF located in the ventral SON. Figure 5 shows tonotopic analyses of two individual SONs. Figure 5A shows the case presented in Figure 4 with CFs of recording sites indicated by colored dots. We tested for a relationship between location and CF by using both linear and log regression functions. In 15 cases, including the two shown in Figure 5A and B, a linear relationship best predicted the tonotopic organization. In two cases a log equation better fit the data, and in two cases no relation was observed (Table 1). These results are comparable to the linear representation of frequency in other auditory brainstem nuclei in chickens (Rubel and Parks, 1975). In the case shown in Figure 5A, the coefficient of determination (r^2) indicated that 85% of the variation in CF could be accounted for by the location of the recording within SON. The case illustrated in Figure 5B had an r^2 value of 0.62 (see Table 1 for all r^2 values). The tonotopic axes, determined by the regression functions, are represented with arrows drawn through the center of mass of the recording sites and pointing to high CF (Fig. 5A,B).

To visually compare the tonotopic organization between cases, all statistically significant tonotopic axes (17 of 19 cases) were overlaid on a single 3D reconstruction of the SON (Fig. 5C). Here, the lengths of the arrows approximate the extent of the SON in that direction sampled in each case. Also, we measured the angles between the dorsal-ventral axis and the tonotopic axes in the medial-lateral (mean ± SD, Θ_{ML}: −4 ± 38°) and anterior-posterior (Θ_{AP}: −12 ± 24°) dimensions (Table 1). In 14 cases the CF was predominantly mapped along the dorsal-ventral axis of the SON; from lower CF in the dorsal SON to higher CF in the ventral SON (Fig. 5C, left and center). This trend was apparent whether recording sites were concentrated in the anterior, posterior, medial, or lateral region of the SON (Fig. 5A,B, Table 1).

Standardized SON is tonotopically organized

Above we demonstrated that individual SONs were tonotopically organized. However, in most subjects we sampled a limited region of the SON. In order to map the tonopic organization of the entire SON, we standardized the reconstructed SONs and the locations of the neuronal recordings and analyzed this combined dataset.

To combine data from all 19 reconstructed SONs, locations of the recording sites were converted into normalized distances along three orthogonal axes in the SON (see Materials

and Methods). These normalized coordinates allowed all recording sites to be mapped in a standardized SON.

Because the presence and arrangement (linear or nonlinear, single or multiple gradients) of the tonotopic organization in SON were unknown, we performed principal component analysis (PCA) on the combined dataset to determine the appropriate dimension(s) to observe the possible tonotopic organization. The first principal component accounted for 72% of the variance in the data (Fig. 6D). Visualizing this component in three spatial dimensions (Fig. 6A-C, gray arrows) revealed that it was dorsoventrally oriented and followed the gradient of CFs in the SON. These results suggest that frequency is organized in a gradient along one dimension in the SON.

To quantitatively model the tonotopic organization in the combined dataset, we performed MRA by using both linear and log equations. A linear equation (Eq. 1) best fit the combined dataset, finding a significant but not strong correlation ($r^2 = 0.62$, $P < 0.01$) between CF and location within the SON. The regression function suggests a predominantly dorsoventrally oriented tonotopic axis in SON (Fig. 6A-C, black arrow). Supplemental Movie 2 shows the 3D standardized SON with CF of recording sites and the orientations of the first principal component and regression function, rotating around the dorsal-ventral axis. Comparing the predicted and measured CFs, we found that error magnitude ($|CF_{predicted} - CF_{measured}|$) varied widely at each position along the calculated tonotopic axis (Fig. 6E). We performed these same analyses on a dataset including only isolated neuronal recording sites (Fig. 6D,E, red). The results of both PCA and MRA were similar to the results obtained from the complete dataset. Both the large error magnitude and the relatively low r^2 value suggest that the frequency map in the SON is not as precise as the tonotopic organization in other brainstem auditory nuclei in the same species (Rubel and Parks, 1975).

Next, we examined the possibility that the relatively low r^2 values reflected particular regions of the SON that did not match the predicted frequency organization. To address this possibility, the standardized SON was sliced into five sections containing approximately the same number of recording sites using isofrequency planes (inset in Fig. 6F). Sections were collapsed along the tonotopic axis into 2D, and MRA showed no significant relation between these 2D locations of recordings and CF ($P > 0.05$ for MRA of all slices). Also, CF was not correlated with medial-lateral (Fig. 6F) or anterior-posterior (Fig. 6G) location in these sections, but varied widely throughout these slices. Because we did not detect a pattern to the distribution of error across SON we did not pursue nonlinear analyses.

To compare the location of regions of SON involved in processing different ranges of stimulus frequencies, we visualized the location of low (CF<1120 Hz, n = 219), intermediate (1120 Hz < CF < 2,460 Hz, n = 233) and high (CF > 2,460 Hz, n = 207) CF neuronal responses (Fig. 7). As expected from the analyses of the tonotopic organization, the low CF sites were densely distributed in the dorsal SON (Fig. 7A), whereas the high CF sites were densely distributed in the ventral SON (Fig. 7C). Intermediate CF sites were densely distributed in a band through the middle of the SON (Fig. 7B). When viewed in the horizontal plane (Figs. 6C, 7, bottom) the CF distribution within these three broad divisions of CF appeared quite random.

Distribution patterns of response patterns in SON

We examined the spatial distribution patterns of isolated neurons with onset or sustained response patterns. Suppressed responders were encountered too infrequently to assess their spatial distribution. As shown in Figure 8A, both onset and sustained responders were located throughout SON. In addition, the distributions of onset and sustained responders were similar across the tonotopic axis derived from the regression function (Fig. 8B). By using MRA, we examined the tonotopic organization of onset and sustained responders separately. Both neuronal types showed a dorsal (low CF) to ventral (high CF) tonotopic organization (Fig. 8C, Table 1). These results suggest that onset and sustained types of neuronal responses are not distributed in separate regions or patterns, but instead are interspersed throughout SON.

Discussion

We investigated the tonotopic organization and neural response properties in the SON, the primary source of inhibitory inputs to auditory nuclei in the avian dorsal brainstem. We generated a quantitative 3D map of the relationship between the characteristic frequency (CF) and anatomical coordinates by using predictive statistical methods. This map is required for future investigation of functional roles of the SON, in particular those involving interactions between frequency representation and coding of other acoustic features. This map contains three main observations: 1) sound frequency is linearly mapped approximately dorsal-ventral across SON; 2) this tonotopic organization is less precise than that of the other nuclei in the auditory brainstem, suggesting that inhibitory function in this avian auditory circuitry does not depend on precise tuning; and 3) neurons with sustained or onset response patterns are interspersed throughout the SON in all CF regions. These findings are consistent with proposed roles of the SON in regulating firing rate and frequency tuning of its targets. In the sections below, we first compare the quantitative mapping methods used in the current study with other quantitative methods that have been applied in topographical mapping. Next we compare physiological properties of SON with other auditory centers in birds in relation to their role in auditory information processing. Finally, we relate SON circuitry to inhibitory function in mammalian auditory brainstems.

Comparison of quantitative mapping methods

This work follows a long history of studies attempting to map frequency tuning and other physiological features of auditory structures (Clopton et al., 1974; Rubel and Parks, 1975; Sanes et al., 1989; Bajo et al., 1999; Cohen and Knudsen, 1999). In these studies, 3D auditory structures were often collapsed along assumed inconsequential dimensions into lower (one or two) dimensional projections from which all analyses were performed. Laminar structures such as sensory epithelium and cortical areas are usually suited for 2D analyses. However, sensory centers in other regions of the brain more often have complex 3D structures. Traditional analyses based on 2D projections of these complex structures are not able to provide complete and accurate knowledge of their organization. Quantitative constructions of topographic maps in 3D, such as the approach we adopted to map the SON, offer a number of advantages: 1) no loss of information from dimension reduction; 2)

visualizing the dataset and model in 3D; 3) creating an expandable database; and 4) comparing structures between experimental groups or between species.

We used two complementary methods, PCA and MRA, to analyze the topography of SON features. Both methods produced similar results from the standardized dataset. A key application of PCA is data analysis of an unknown, but potentially low-dimensional system. In the current study, PCA produced low-dimensional reductions of the tonotopic organization from seemingly complex data collected in the SON, when equations governing this organization were not known.

In addition to PCA, we used MRA to examine the relation between location and frequency tuning in the SON. Generally, in different auditory nuclei this relationship can be best described by different regression functions, such as linear, log, or power (Clopton et al., 1974). Our results demonstrated that the tonotopic organization of SON was best fit by linear functions, similar to other studied auditory nuclei in chicken (Rubel and Parks, 1975; Heil and Scheich, 1985). This linear relationship, as opposed to a log relationship often observed in auditory centers, is probably a consequence of the limited frequency range of hearing in chickens (Gray and Rubel, 1985; Saunders and Salvi, 1993) relative to most mammals (Masterton et al., 1969).

3D tonotopic map of SON

Most individual cases showed recording locations organized tonotopically from low frequencies in the dorsal SON to high frequencies in the ventral SON. The analyses of two cases showed no tonotopic organization, probably due to a limited number of recording sites in one case (100810) and a few aberrant recording sites in the other case (110228). When the standardized SON was analyzed, the multilinear regression function accounted for 60% of the variability in the dataset, an indicator of the precision of this topographical map. This degree of precision is notably less than the coefficient of determination (r^2), calculated from the basilar papilla, NL, nucleus magnocellularis (NM), and Field L in chickens (Rubel and Parks, 1975; Ryals and Rubel, 1982; Heil and Scheich, 1985; Manley et al., 1987), but similar to those quantified in the lateral superior olive, inferior colliculus, medial geniculate nucleus, and auditory cortex in cat (Clopton et al., 1974) and in Field L complex in canary (Terleph et al., 2006). Finally, we found that neurons with the two most common response types, sustained and onset, are interspersed throughout the SON. Each type forms a complete tonotopic representation, and these maps show similar spatial arrangements. Thus, the SON appears to process at least two types of information in parallel.

Two features common to all auditory nuclei studied in the bird brainstem including the SON are: 1) that only a single frequency representation is found for each nucleus (Rubel and Parks, 1975; Koppl, 2001); and 2) that the tonotopic map preserves the topographic organization of the sensory epithelium without magnification or compression (Ryals and Rubel, 1982; Manley et al., 1987).

Possible functions of SON

Firing patterns of SON neurons to ipsilateral tones appear to be shaped primarily by the inputs from the NA, one of two main excitatory inputs to the SON. First, physiological

response patterns of SON neurons closely resemble those of NA neurons. Both nuclei include sustained and onset responders and diverse frequency-level response maps (Sachs et al., 1978; Moiseff and Konishi, 1983; Warchol and Dallos, 1990; Lachica et al., 1994; Carr and Soares, 2002; Soares et al., 2002; Koppl and Carr, 2003; Fukui et al., 2010; Coleman et al., 2011). Second, response thresholds in SON are similar to CF-matched NA neurons, whereas NM neurons may have slightly higher thresholds (Sachs et al., 1978; Warchol and Dallos, 1990; Coleman et al., 2011). Although the SON most closely resembles the NA physiologically, we cannot exclude contributions from the NL. It is possible that sustained responders in the SON may derive their responses from NL inputs. NL neurons, in turn, inherit their monaural physiological characteristics from NM neurons, which include primary-like response patterns and simple V-shaped tuning curves. Also, we did not assess the binaural response properties of SON neurons in this study, which could reveal a currently unexplored contribution from NL's projection to SON response properties.

One proposed function of the SON is lateral sharpening of frequency tuning in its target neurons within the NM, NA, and NL. An in vivo physiological study revealed that inhibitory input to the NM is more broadly tuned than excitatory input to the NM (Fukui et al., 2010). Whether this broadly tuned inhibition results from a few broadly tuned SON inputs or the convergence of many narrower tuned inputs remains to be determined. Because frequency selectivity (e.g., Q10 dB values) varies widely between SON neurons, encompassing the range of Q10 dB values reported for NA and NM neurons (Warchol and Dallos, 1990), the convergence of SON inputs to the NM accounting for the broad tuning cannot be accurately predicted from the data available. In the NL, the breadth of inhibitory tuning remains unknown; however, anatomical studies demonstrated a broad topographic organization of the SON-NL projection in marked contrast to the NMNL projections, which innervate highly restricted regions of the tonotopic axis (Young and Rubel, 1983; Tabor et al., 2011). This projection pattern suggests an anatomical substrate for lateral sharpening of frequency tuning in NL neurons.

How the diverse response properties of SON neurons to pure tone stimuli affect the neuronal activity in this circuit remains unknown. The majority of SON neurons show a sustained response to tones with their firing rate reflecting stimulus intensity. This pattern is well suited to regulate the gain of the circuit, a function that has been implied for SON (Pena et al., 1996; Burger et al., 2005; Dasika et al., 2005). In addition, many neurons with sustained responses show phase-locking, which may provide temporally patterned inhibition to the network (Coleman et al., 2011). Timed inhibition is important for computing interaural timing differences in the gerbil medial superior olive (MSO) (Brand et al., 2002; Grothe, 2003); however, its role in the avian auditory brainstem has not been tested.

Comparison with mammals

The mammalian auditory system does not appear to have an exact homolog or analog to the SON. Instead, mammals have multiple nuclei that provide inhibition to the auditory brainstem and the inner ear. These nuclei, which may include the medial nucleus of the trapezoid body (MNTB) and a number of periolivary nuclei, provide a similar range of functions as the SON in birds. Our current view is that the SON enables binaural balancing

of neural activity (Burger et al., 2005; Dasika et al., 2005; Fukui et al., 2010; for review, see Burger et al., 2011) that is essential for brainstem processing of low-frequency binaural information used for sound localization. In addition, the SON provides feedback inhibition to the NL and the cochlear nuclei (Lachica et al., 1994; Yang et al., 1999; Monsivais et al., 2000; Burger et al., 2005), and feed-forward inhibition to the lateral lemniscus (LL) and midbrain (Conlee and Parks, 1986; Westerberg and Schwarz, 1995; Wild et al., 2009). In rodents, binaural balancing is performed by the lateral olivocochlear efferents (Groff and Liberman, 2003; Darrow et al., 2006).

Feedback inhibition to all subdivisions of the mammalian cochlear nucleus is provided by glycinergic and GABAergic input from periolivary regions, in particular, the contralateral ventral nucleus of the trapezoid body, and the ipsilateral MNTB and lateral nucleus of the trapezoid body (LNTB) (Adams, 1983; Spangler et al., 1985; Schofield, 1994; Warr and Beck, 1996; Ostapoff et al., 1997). Inhibition to MSO (analogous to NL) is provided by MNTB and LNTB (Cant and Hyson, 1992; Grothe and Sanes, 1993). Feed-forward inhibition to LL and the auditory midbrain is provided by a combination of the various nuclei, including the MNTB, LNTB (Yavuzoglu et al., 2010), and superior periolivary nucleus (also named the dorsomedial periolivary nucleus) in mammals (Kadner and Berrebi, 2008; Saldana et al., 2009; Kopp-Scheinpflug et al., 2011). The comparatively simple organization of inhibition in the avian auditory brainstem makes this an appealing model for studying the roles of inhibition in auditory processing in vertebrates.

Supplementary Material

Refer to Web version on PubMed Central for supplementary material.

Acknowledgments

We thank Dr. Yuan Wang for critical reading of the manuscript; Dr. Rachel Wong, Matthew Fischl, Stefan Oline, and Sonia Weimann for discussion; Dr. Adrienne Fairhall for help with analyses; David Schneider and Dr. Sarah Woolley for PostHawk software; and Brandon Warren for Spike software.

Grant sponsor: National Institute on Deafness and Other Communication Disorders, National Institutes of Health; Grant numbers: DC008989 (to R.M.B.), DC03829 and DC04661 (to E.W.R.), and T32 DC005361 (to the University of Washington).

Literature Cited

Adams JC. Multipolar cells in the ventral cochlear nucleus project to the dorsal cochlear nucleus and the inferior colliculus. Neurosci Lett. 1983; 37:205–208. [PubMed: 6888799]

Bajo VM, Merchan MA, Malmierca MS, Nodal FR, Bjaalie JG. Topographic organization of the dorsal nucleus of the lateral lemniscus in the cat. J Comp Neurol. 1999; 407:349–366. [PubMed: 10320216]

Brand A, Behrend O, Marquardt T, McAlpine D, Grothe B. Precise inhibition is essential for microsecond interaural time difference coding. Nature. 2002; 417:543–547. [PubMed: 12037566]

Burger RM, Cramer KS, Pfeiffer JD, Rubel EW. Avian superior olivary nucleus provides divergent inhibitory input to parallel auditory pathways. J Comp Neurol. 2005; 481:6–18. [PubMed: 15558730]

Burger RM, Fukui I, Ohmori H, Rubel EW. Inhibition in the balance: binaurally coupled inhibitory feedback in sound localization circuitry. J Neurophysiol. 2011; 106:4–14. [PubMed: 21525367]

Cant NB, Hyson RL. Projections from the lateral nucleus of the trapezoid body to the medial superior olivary nucleus in the gerbil. Hear Res. 1992; 58:26–34. [PubMed: 1559903]

Carr CE, Soares D. Evolutionary convergence and shared computational principles in the auditory system. Brain Behav Evol. 2002; 59:294–311. [PubMed: 12207085]

Clopton BM, Winfield JA, Flammino FJ. Tonotopic organization: review and analysis. Brain Res. 1974; 76:1–20. [PubMed: 4367399]

Cohen YE, Knudsen EI. Maps versus clusters: different representations of auditory space in the midbrain and forebrain. Trends Neurosci. 1999; 22:128–135. [PubMed: 10199638]

Coleman WL, Fischl MJ, Weimann SR, Burger RM. GABAergic and glycinergic inhibition modulate monaural auditory response properties in the avian superior olivary nucleus. J Neurophysiol. 2011; 105:2405–2420. [PubMed: 21368002]

Conlee JW, Parks TN. Origin of ascending auditory projections to the nucleus mesencephalicus lateralis pars dorsalis in the chicken. Brain Res. 1986; 367:96–113. [PubMed: 3697720]

Darrow KN, Simons EJ, Dodds L, Liberman MC. Dopaminergic innervation of the mouse inner ear: evidence for a separate cytochemical group of cochlear efferent fibers. J Comp Neurol. 2006; 498:403–414. [PubMed: 16871528]

Dasika VK, White JA, Carney LH, Colburn HS. Effects of inhibitory feedback in a network model of avian brain stem. J Neurophysiol. 2005; 94:400–414. [PubMed: 15744007]

Fukui I, Burger RM, Ohmori H, Rubel EW. GABAergic inhibition sharpens the frequency tuning and enhances phase locking in chicken nucleus magnocellularis neurons. J Neurosci. 2010; 30:12075–12083. [PubMed: 20826670]

Gray L, Rubel EW. Development of absolute thresholds in chickens. J Acoust Soc Am. 1985; 77:1162–1172. [PubMed: 3980868]

Groff JA, Liberman MC. Modulation of cochlear afferent response by the lateral olivocochlear system: activation via electrical stimulation of the inferior colliculus. J Neurophysiol. 2003; 90:3178–3200. [PubMed: 14615429]

Grothe B. New roles for synaptic inhibition in sound localization. Nat Rev Neurosci. 2003; 4:540–550. [PubMed: 12838329]

Grothe B, Sanes DH. Bilateral inhibition by glycinergic afferents in the medial superior olive. J Neurophysiol. 1993; 69:1192–1196. [PubMed: 8492158]

Heil P, Scheich H. Quantitative analysis and two-dimensional reconstruction of the tonotopic organization of the auditory field L in the chick from 2-deoxyglucose data. Exp Brain Res. 1985; 58:532–543. [PubMed: 4007092]

Huang ZJ, Di Cristo G, Ango F. Development of GABA innervation in the cerebral and cerebellar cortices. Nat Rev Neurosci. 2007; 8:673–686. [PubMed: 17704810]

Kadner A, Berrebi AS. Encoding of temporal features of auditory stimuli in the medial nucleus of the trapezoid body and superior paraolivary nucleus of the rat. Neuroscience. 2008; 151:868–887. [PubMed: 18155850]

Kim G, Kandler K. Elimination and strengthening of glycinergic/GABAergic connections during tonotopic map formation. Nat Neurosci. 2003; 6:282–290. [PubMed: 12577063]

Kopp-Scheinpflug C, Tozer AJ, Robinson SW, Tempel BL, Hennig MH, Forsythe ID. The sound of silence: ionic mechanisms encoding sound termination. Neuron. 2011; 71:911–925. [PubMed: 21903083]

Koppl C. Tonotopic projections of the auditory nerve to the cochlear nucleus angularis in the barn owl. J Assoc Res Otolaryngol. 2001; 2:41–53. [PubMed: 11545149]

Koppl C, Carr CE. Computational diversity in the cochlear nucleus angularis of the barn owl. J Neurophysiol. 2003; 89:2313–2329. [PubMed: 12612008]

Kuba H, Yamada R, Fukui I, Ohmori H. Tonotopic specialization of auditory coincidence detection in nucleus laminaris of the chick. J Neurosci. 2005; 25:1924–1934. [PubMed: 15728832]

Kuo SP, Bradley LA, Trussell LO. Heterogeneous kinetics and pharmacology of synaptic inhibition in the chick auditory brainstem. J Neurosci. 2009; 29:9625–9634. [PubMed: 19641125]

Lachica EA, Rubsamen R, Rubel EW. GABAergic terminals in nucleus magnocellularis and laminaris originate from the superior olivary nucleus. J Comp Neurol. 1994; 348:403–418. [PubMed: 7844255]

Manley GA, Brix J, Kaiser A. Developmental stability of the tonotopic organization of the chick's basilar papilla. Science. 1987; 237:655–656. [PubMed: 3603046]

Masterton B, Heffner H, Ravizza R. The evolution of human hearing. J Acoust Soc Am. 1969; 45:966–985. [PubMed: 5791616]

Moiseff A, Konishi M. Neuronal and behavioral sensitivity to binaural time differences in the owl. J Neurosci. 1981; 1:40–48. [PubMed: 7346557]

Moiseff A, Konishi M. Binaural characteristics of units in the owl's brainstem auditory pathway: precursors of restricted spatial receptive fields. J Neurosci. 1983; 3:2553–2562. [PubMed: 6655499]

Monsivais P, Yang L, Rubel EW. GABAergic inhibition in nucleus magnocellularis: implications for phase locking in the avian auditory brainstem. J Neurosci. 2000; 20:2954–2963. [PubMed: 10751448]

Nishino E, Ohmori H. The modulation by intensity of the processing of interaural timing cues for localizing sounds. Mol Neurobiol. 2009; 40:157–165. [PubMed: 19593674]

Ostapoff EM, Benson CG, Saint Marie RL. GABA- and glycine-immunoreactive projections from the superior olivary complex to the cochlear nucleus in guinea pig. J Comp Neurol. 1997; 381:500–512. [PubMed: 9136806]

Pena JL, Viete S, Albeck Y, Konishi M. Tolerance to sound intensity of binaural coincidence detection in the nucleus laminaris of the owl. J Neurosci. 1996; 16:7046–7054. [PubMed: 8824340]

Rubel EW, Parks TN. Organization and development of brain stem auditory nuclei of the chicken: tonotopic organization of n. magnocellularis and n. laminaris. J Comp Neurol. 1975; 164:411–433. [PubMed: 1206127]

Ryals BM, Rubel EW. Patterns of hair cell loss in chick basilar papilla after intense auditory stimulation. Frequency organization. Acta Otolaryngol. 1982; 93:205–210. [PubMed: 7064706]

Sachs MB, Sinnott JM, Hienz RD. Behavioral and physiological studies of hearing in birds. Fed Proc. 1978; 37:2329–2335. [PubMed: 98352]

Saldana E, Aparicio MA, Fuentes-Santamaria V, Berrebi AS. Connections of the superior paraolivary nucleus of the rat: projections to the inferior colliculus. Neuroscience. 2009; 163:372–387. [PubMed: 19539725]

Sanes DH, Friauf E. Development and influence of inhibition in the lateral superior olivary nucleus. Hear Res. 2000; 147:46–58. [PubMed: 10962172]

Sanes DH, Merickel M, Rubel EW. Evidence for an alteration of the tonotopic map in the gerbil cochlea during development. J Comp Neurol. 1989; 279:436–444. [PubMed: 2918079]

Saunders SS, Salvi RJ. Psychoacoustics of normal adult chickens: thresholds and temporal integration. J Acoust Soc Am. 1993; 94:83–90. [PubMed: 8354763]

Schofield BR. Projections to the cochlear nuclei from principal cells in the medial nucleus of the trapezoid body in guinea pigs. J Comp Neurol. 1994; 344:83–100. [PubMed: 7520457]

Smith DJ, Rubel EW. Organization and development of brain stem auditory nuclei of the chicken: dendritic gradients in nucleus laminaris. J Comp Neurol. 1979; 186:213–239. [PubMed: 447882]

Soares D, Chitwood RA, Hyson RL, Carr CE. Intrinsic neuronal properties of the chick nucleus angularis. J Neurophysiol. 2002; 88:152–162. [PubMed: 12091541]

Spangler KM, Warr WB, Henkel CK. The projections of principal cells of the medial nucleus of the trapezoid body in the cat. J Comp Neurol. 1985; 238:249–262. [PubMed: 4044914]

Tabor KM, Wong RO, Rubel EW. Topography and morphology of the inhibitory projection from superior olivary nucleus to nucleus laminaris in chickens (*Gallus gallus*). J Comp Neurol. 2011; 519:358–375. [PubMed: 21165979]

Takahashi T, Moiseff A, Konishi M. Time and intensity cues are processed independently in the auditory system of the owl. J Neurosci. 1984; 4:1781–1786. [PubMed: 6737040]

Terleph TA, Mello CV, Vicario DS. Auditory topography and temporal response dynamics of canary caudal telencephalon. J Neurobiol. 2006; 66:281–292. [PubMed: 16329130]

Thevenaz P, Ruttimann UE, Unser M. A pyramid approach to subpixel registration based on intensity. IEEE Trans Image Process. 1998; 7:27–41. [PubMed: 18267377]

Tsuchitani C, Boudreau JC. Single unit analysis of cat superior olive S segment with tonal stimuli. J Neurophysiol. 1966; 29:684–697. [PubMed: 5966430]

Warchol ME, Dallos P. Neural coding in the chick cochlear nucleus. J Comp Physiol A. 1990; 166:721–734. [PubMed: 2341992]

Warr WB, Beck JE. Multiple projections from the ventral nucleus of the trapezoid body in the rat. Hear Res. 1996; 93:83–101. [PubMed: 8735070]

Westerberg BD, Schwarz DW. Connections of the superior olive in the chicken. J Otolaryngol. 1995; 24:20–30. [PubMed: 7769641]

Wild JM, Krutzfeldt NO, Kubke MF. Connections of the auditory brainstem in a songbird, *Taeniopygia guttata*. III. Projections of the superior olive and lateral lemniscal nuclei. J Comp Neurol. 2009; 518:2149–2167. [PubMed: 20394063]

Yang L, Monsivais P, Rubel EW. The superior olivary nucleus and its influence on nucleus laminaris: a source of inhibitory feedback for coincidence detection in the avian auditory brainstem. J Neurosci. 1999; 19:2313–2325. [PubMed: 10066281]

Yavuzoglu A, Schofield BR, Wenstrup JJ. Substrates of auditory frequency integration in a nucleus of the lateral lemniscus. Neuroscience. 2010; 169:906–919. [PubMed: 20451586]

Young SR, Rubel EW. Frequency-specific projections of individual neurons in chick brainstem auditory nuclei. J Neurosci. 1983; 3:1373–1378. [PubMed: 6864252]

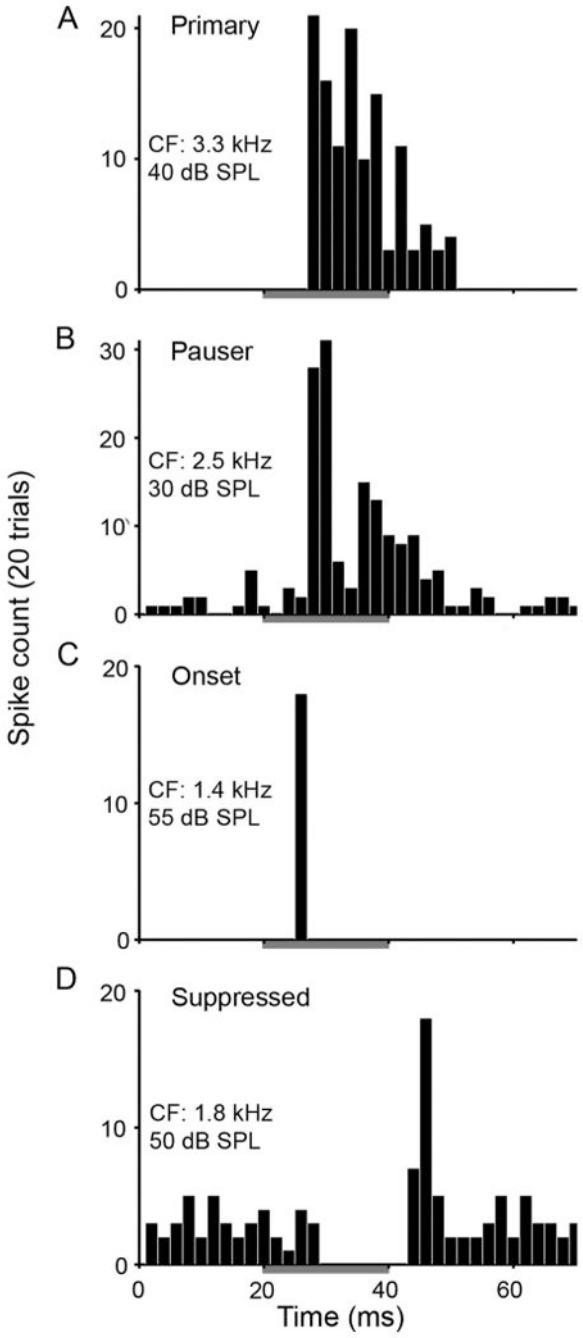

Figure 1.

SON neurons show three classes of response patterns to ipsilateral tones. Post-stimulus time histograms constructed from responses to 20 presentations of CF tones at 20 dB above response threshold. See histograms for CF of neurons and stimulus intensity. **A–D:** Histograms show sustained (including primary-like [A] and pauser-like [B] types), onset (C), and suppressed (D) firing patterns. Gray bars indicate 20-ms tone presentations with 5-ms rise and fall times for triangle-shaped envelopes. Binwidth: 2 ms.

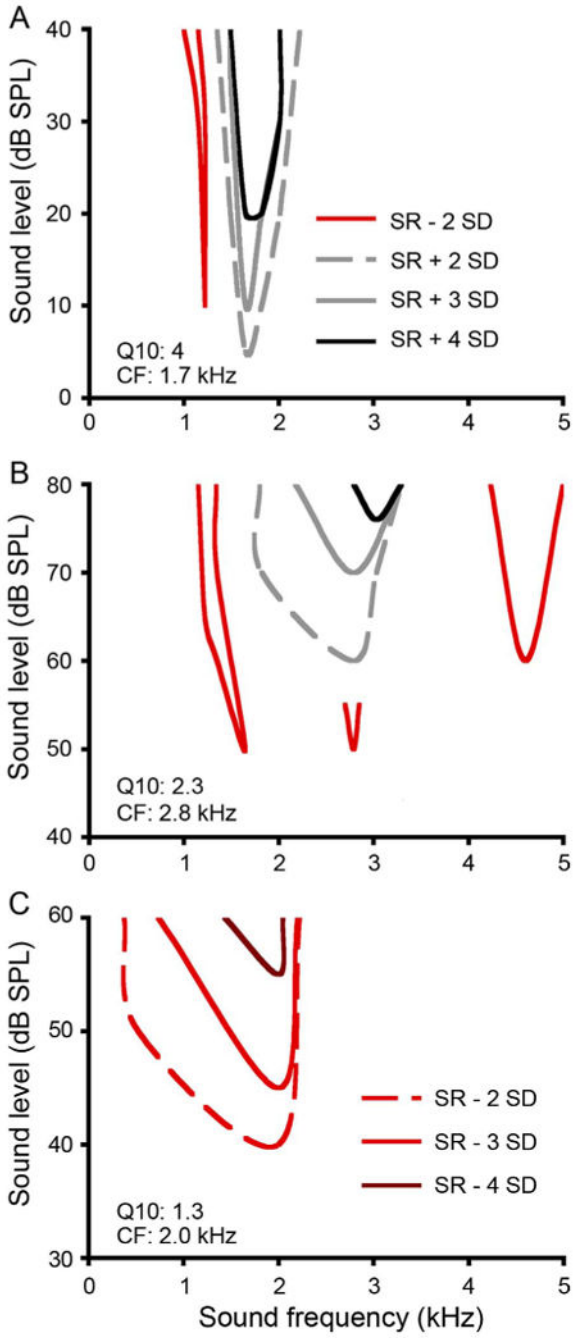

Figure 2.

SON neurons show complex frequency response maps to ipsilateral tones. **A,B:** Response maps of two sustained responders. Contours represent boundaries of excitatory responses 2 SD above spontaneous firing rate (SR) indicated by gray dashed lines (the criterion used to determine response threshold at CF), 3 SD above SR (gray solid lines), and 4 SD above SR (black lines). Complex patterns of frequency or level-dependent suppression of responses are indicated by red lines (2 SD below SR). **C:** Response map of a suppressed responder. Contours represent boundaries of suppression 2 SD below SR (red dashed line; the criterion

used to determine response threshold at CF), 3 SD below SR (red solid line), and 4 SD below SR (dark red line). All responses were assessed with 20- or 40-ms tones with 5-ms rise and fall times for triangle-shaped envelopes. Abbreviations: CF, characteristic frequency; SR, spontaneous firing rate.

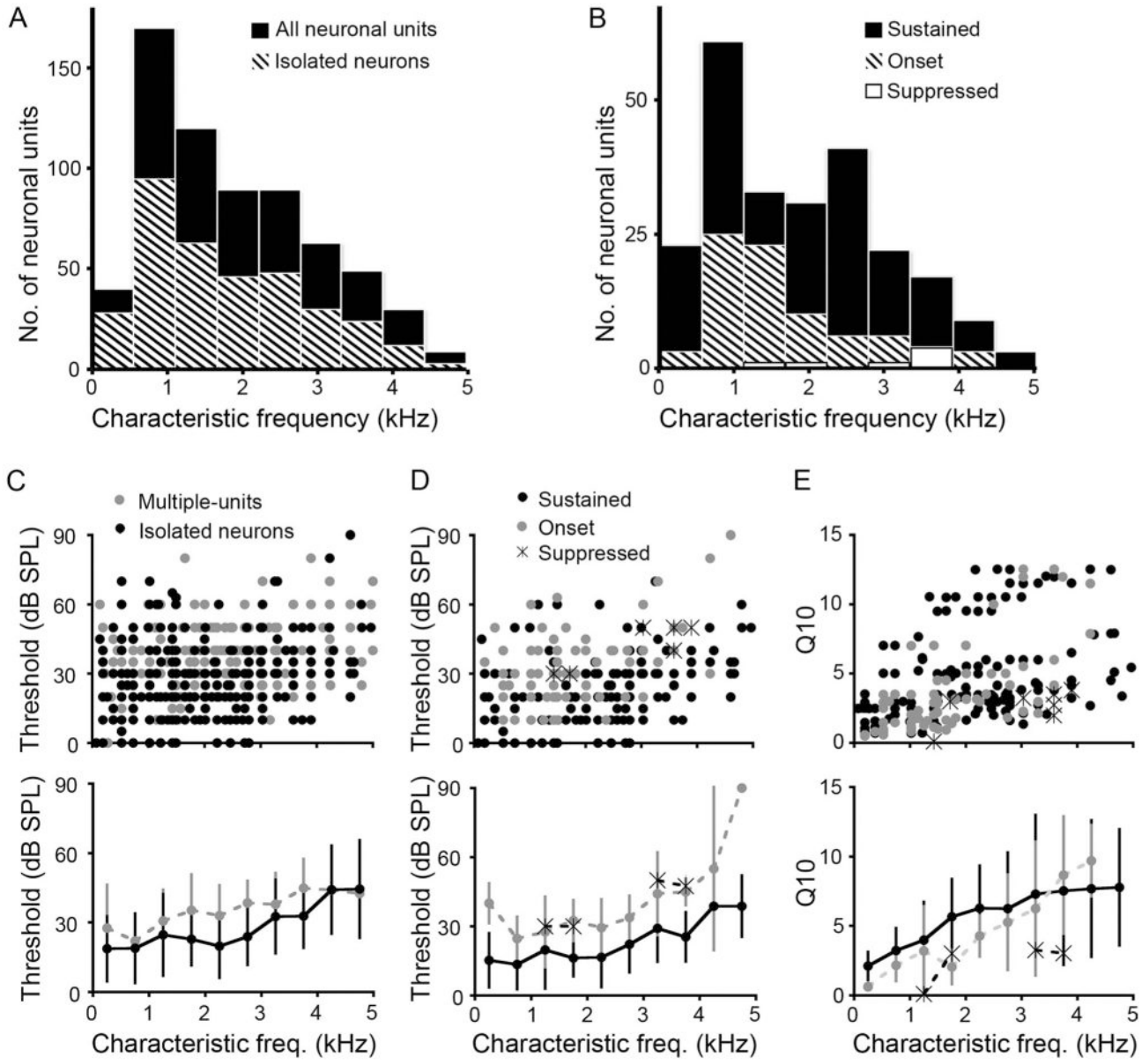

Figure 3.

Heterogeneity of response properties to ipsilateral tones is expressed across CF in SON. **A:** Histogram of CFs for all neuronal responses (black) (mean ± SD, CF: 1,947 ± 1,198 Hz, n = 659) and isolated neuronal responses (striped; 1,834 ± 1,170 Hz, n = 349). **B:** Histogram of CFs for sustained (black; 1,870 ± 1,214 Hz, n = 233), onset (striped; 1,690 ± 1,031 Hz, n = 80), and suppressed (white; 2,975 ± 994 Hz, n = 7) isolated neuronal responses (binwidth: 600 Hz). **C:** Scatterplot showing response threshold as a function of CF for each recording site (top panel) and mean thresholds shown below for both multiple units (gray) and isolated neurons (black; multiple-unit threshold: 34 ± 15 dB, n = 310; isolated neurons: 24 ± 16 dB). **D:** *Top panel*, scatterplot showing distribution of thresholds as a function of CF for

sustained (black dots), onset (gray dots), and suppressed (asterisks) neurons. *Bottom panel* shows that overall, mean thresholds for both onset and sustained neurons increase with CF. **E:** Scatterplot (top) and mean ± SD (bottom) Q10 values showing a mild increase as a function of CF for each response type (Q10 values: sustained, 5 ± 3.6; onset, 3.7 ± 3.4; suppressed, 2.6 ± 1.3). C–E bottom, binwidth: 500 Hz.

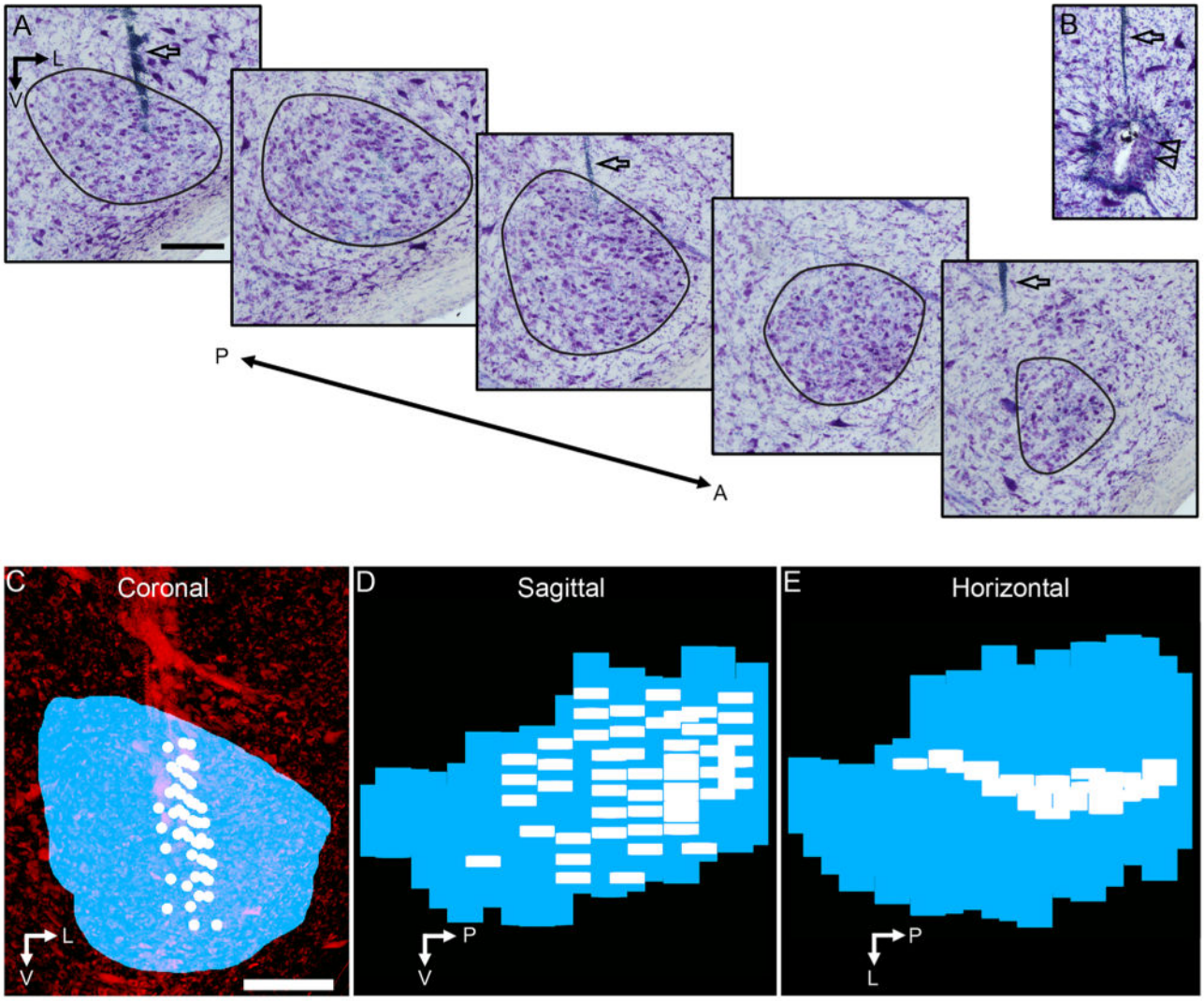

Figure 4.

3D reconstruction of the SON and locations of neuronal recordings. **A:** Series of Nissl-stained sections through the SON; black lines define SON borders. **B:** Electrolytic lesion site (double arrowheads) used to map recording sites to tissue. Open arrows (in A and B) indicate electrode tracks. **C–E:** 3D reconstruction of the SON (blue) and location of neuronal recordings (white) shown in coronal (C), sagittal (D), and horizontal (E) views. C shows the ventral brainstem stained for Nissl substance (red). Abbreviations: A, anterior; L, lateral; P, posterior; V, ventral. Scale bars = 200 μm in A (applies to A, B); in C (applies to C–E).

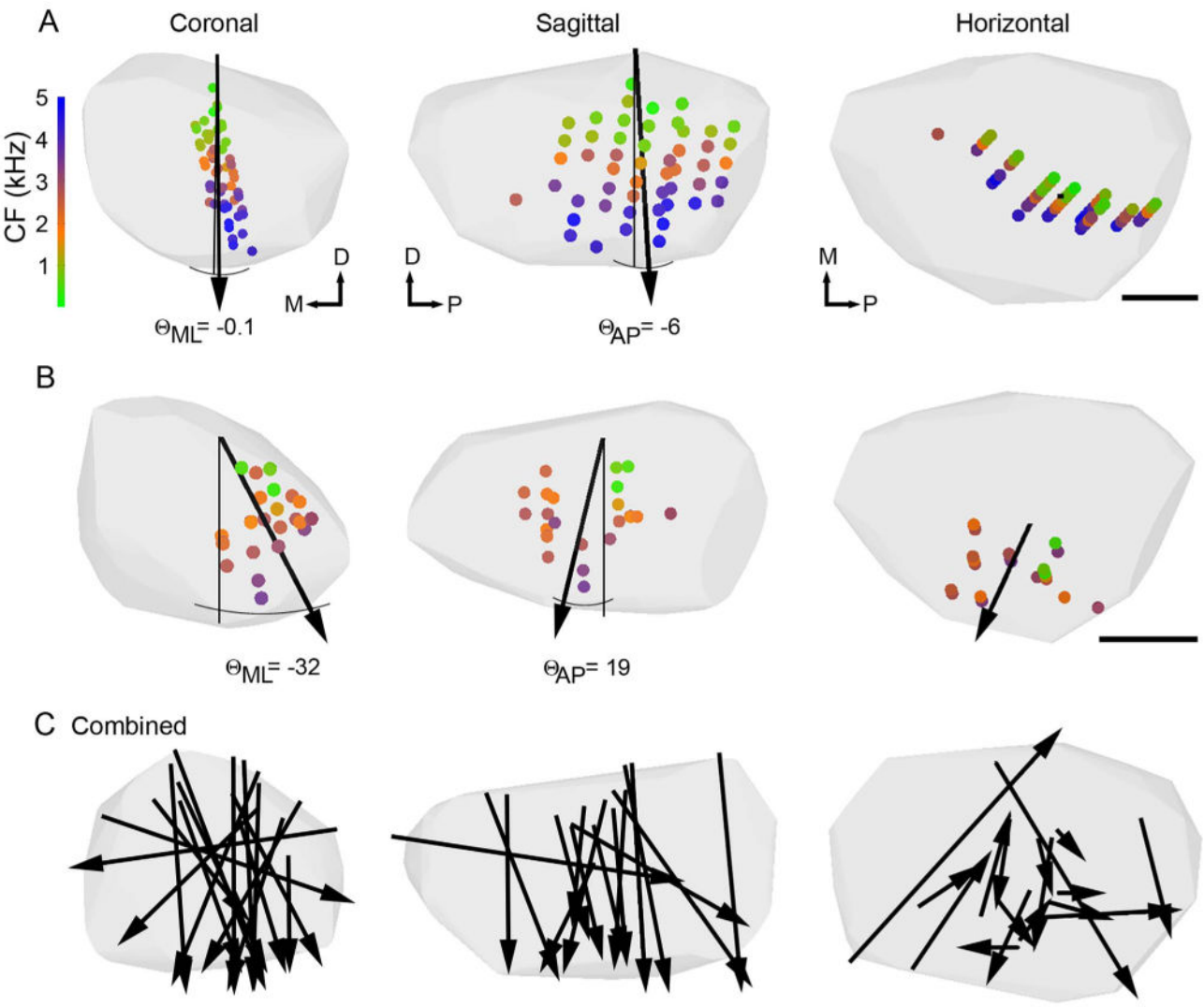

Figure 5.

Individual SON reconstructions show tonotopic organization. Coronal, sagittal and horizontal views of individual SON reconstructions indicated by the gray hulls. **A,B:** Small circles show locations of neuronal recordings color-coded to represent CF (color scale at left). Black arrows show orientation of tonotopic axes derived from MRA. Arrowheads point toward high CFs. Angles between the dorsal-ventral axes (thin black lines) and tonotopic axes in the medial-lateral (Θ_{ML}) and anterior-posterior (Θ_{AP}) dimensions are indicated. Θ values for all cases are listed in Table 1. A shows case 100811 with 51 recordings sites, the same SON reconstruction presented in Figure 4. B shows case 100729 with 24 recordings sites. **C:** Coronal, sagittal, and horizontal views with arrows indicating predicted tonotopic axes from individual SONs (n = 17 of 19) combined on a single SON reconstruction. Each arrow intersects the center of mass of the recording sites in its case. Lengths of arrows approximate the extent of the SON in that direction sampled in each case. Abbreviations: CF, characteristic frequency; D, dorsal; M, medial; P, posterior. Scale bar = 200 μm in A,B.

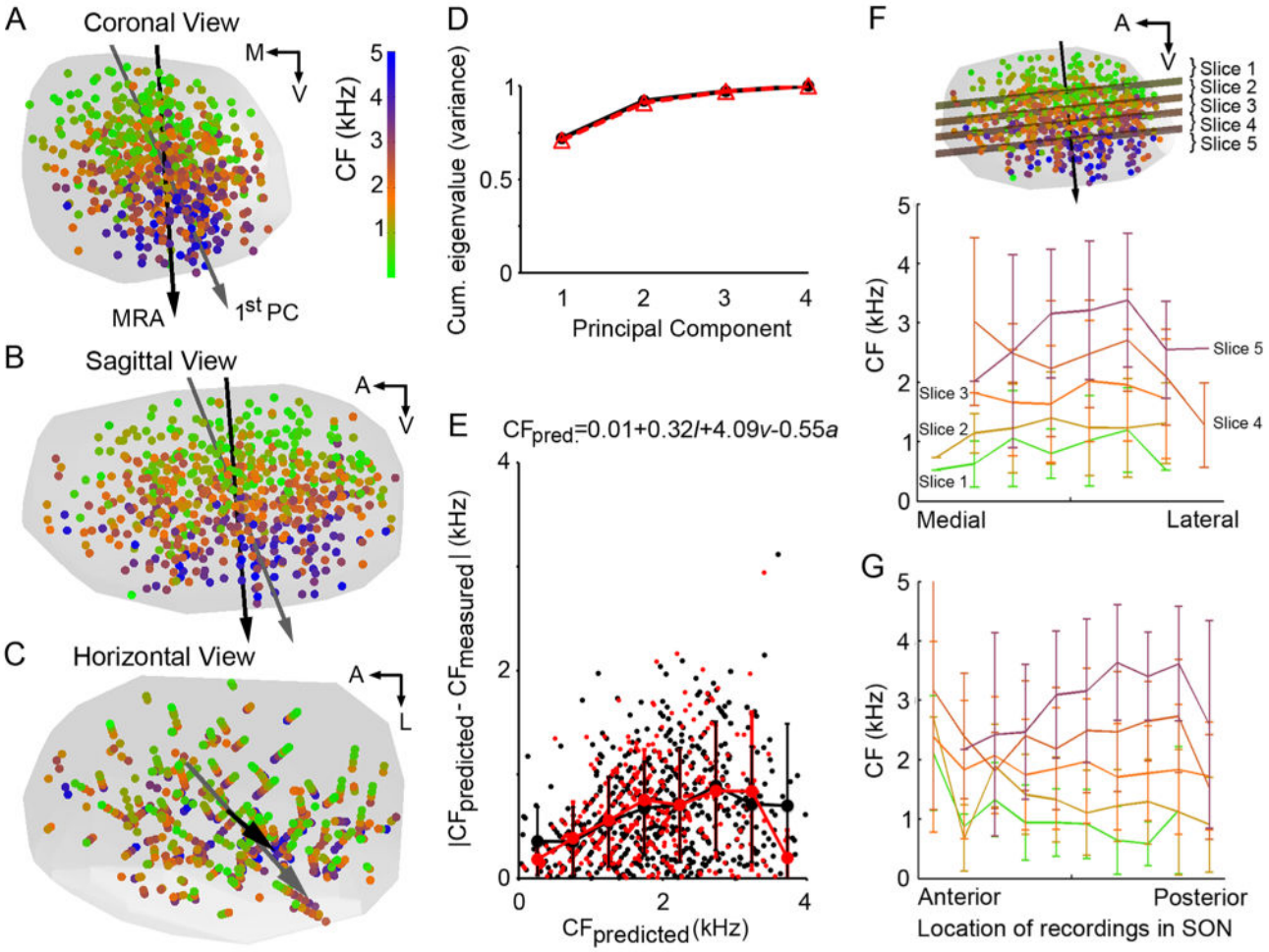

Figure 6.

Standardized SON with all recording sites superimposed shows a linear tonotopic organization. **A-C:** Recording sites (circles) from 19 animals combined on a standardized SON (gray hull) and presented in coronal (A), sagittal (B), and horizontal (C) views. Sites color-coded by CF (color scale in A). Orientation of regression function (black arrows) and first principal component (gray arrows) pointing to high CF regions. Both analyses show dorsal-ventral tonotopic organization across the SON. **D:** Cumulative eigenvalues from PCA performed on complete set of recordings sites (solid black line) or sites of isolated neuronal recordings (triangles, dashed red line). The first principal component accounts for 72% (all sites) or 71% (isolated neuronal sites) of the variance of these distributions. **E:** Magnitude of error of estimate ($|CF_{predicted} - CF_{measured}|$) versus predicted CF determined by MRA. MRA performed on all recording sites (black circles) and isolated neuronal sites (red circles). Mean ± SD shown as a function of predicted CF (binwidth: 500 Hz). Black lines connect mean errors of all recordings. Red lines connect mean errors of isolated neuronal recordings. See E for multilinear regression equation, where CF_{pred}. is the characteristic frequency in kHz, / is the normalized medial-lateral coordinate (lateral edge is 1), *v* is the normalized dorsal-ventral coordinate (ventral edge is 1), and a is the normalized anterior-posterior coordinate (anterior edge is 1). **F,G:** Planes orthogonal to the multilinear regression function

dividing SON sites into five slices (see inset in F) encompassing the following CF ranges: 1) $CF_{predicted}$ < 1,204 Hz, n = 132 sites; 2) 1,204 Hz < $CF_{predicted}$ < 1,698 Hz, n = 131; 3) 1,698 Hz < $CF_{predicted}$ < 2,129 Hz, n = 131; 4) 2,129 Hz < $CF_{predicted}$ < 2,632 Hz, n = 131; 5) 2,632 Hz < $CF_{predicted}$, n = 134. CF versus medial-lateral (F) or anterior-posterior (G) location in the SON plotted for each slice. Mean ± SD shown for bins of 10% of total dimensional distance. Abbreviations: CF, characteristic frequency; A, anterior; L, lateral; M, medial; V, ventral.

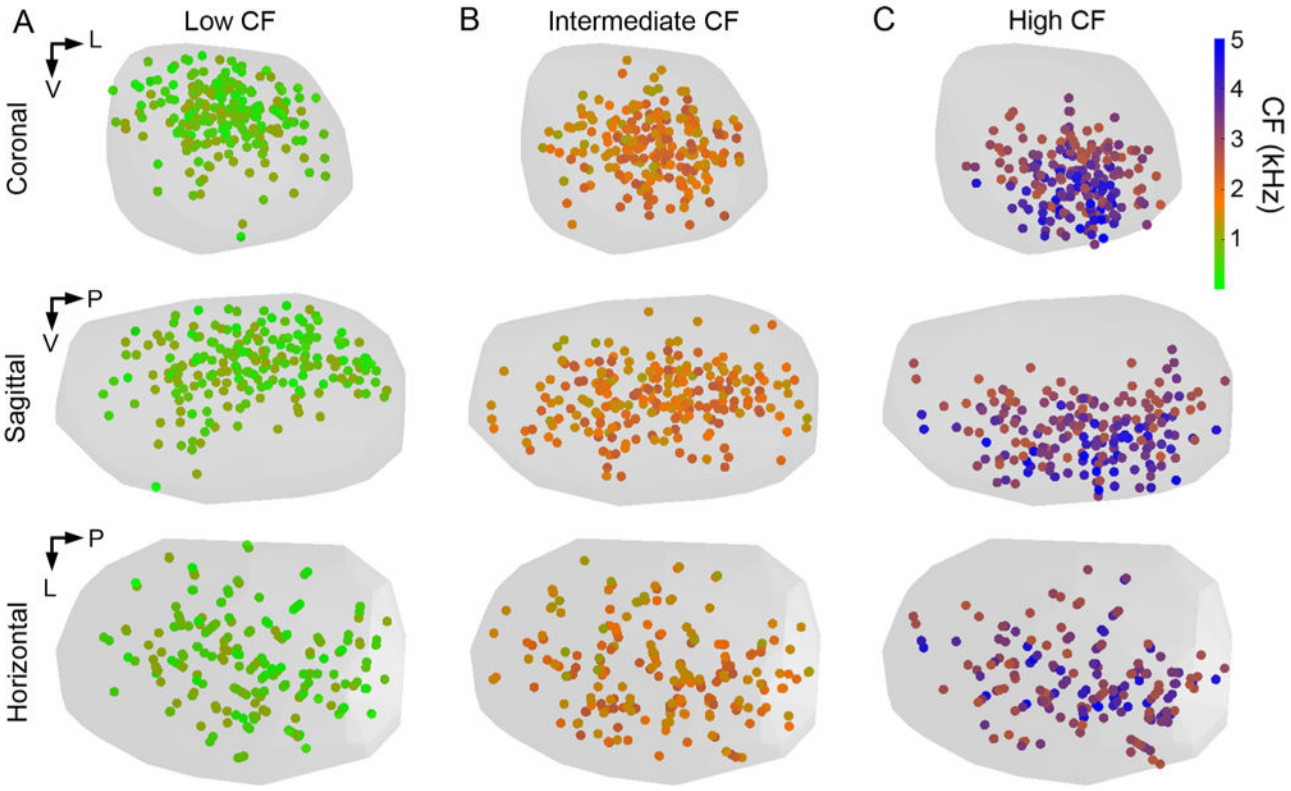

Figure 7.

Distributions of low, intermediate, and high CF recording sites are separated in the standardized SON. Circles show locations of neuronal recordings color-coded to represent CF (color scale at right). **A:** Standardized SON populated with the locations of low CF (CF < 1,120 Hz, n = 219) recording sites shown from the coronal (top), sagittal (middle), and horizontal (bottom) views. **B,C:** Locations of intermediate CF (1,120 Hz < CF < 2,460 Hz, n = 233) and high CF (CF > 2,460 Hz, n = 207) recordings sites, respectively. Abbreviations: CF, characteristic frequency; L, lateral; P, posterior; V, ventral.

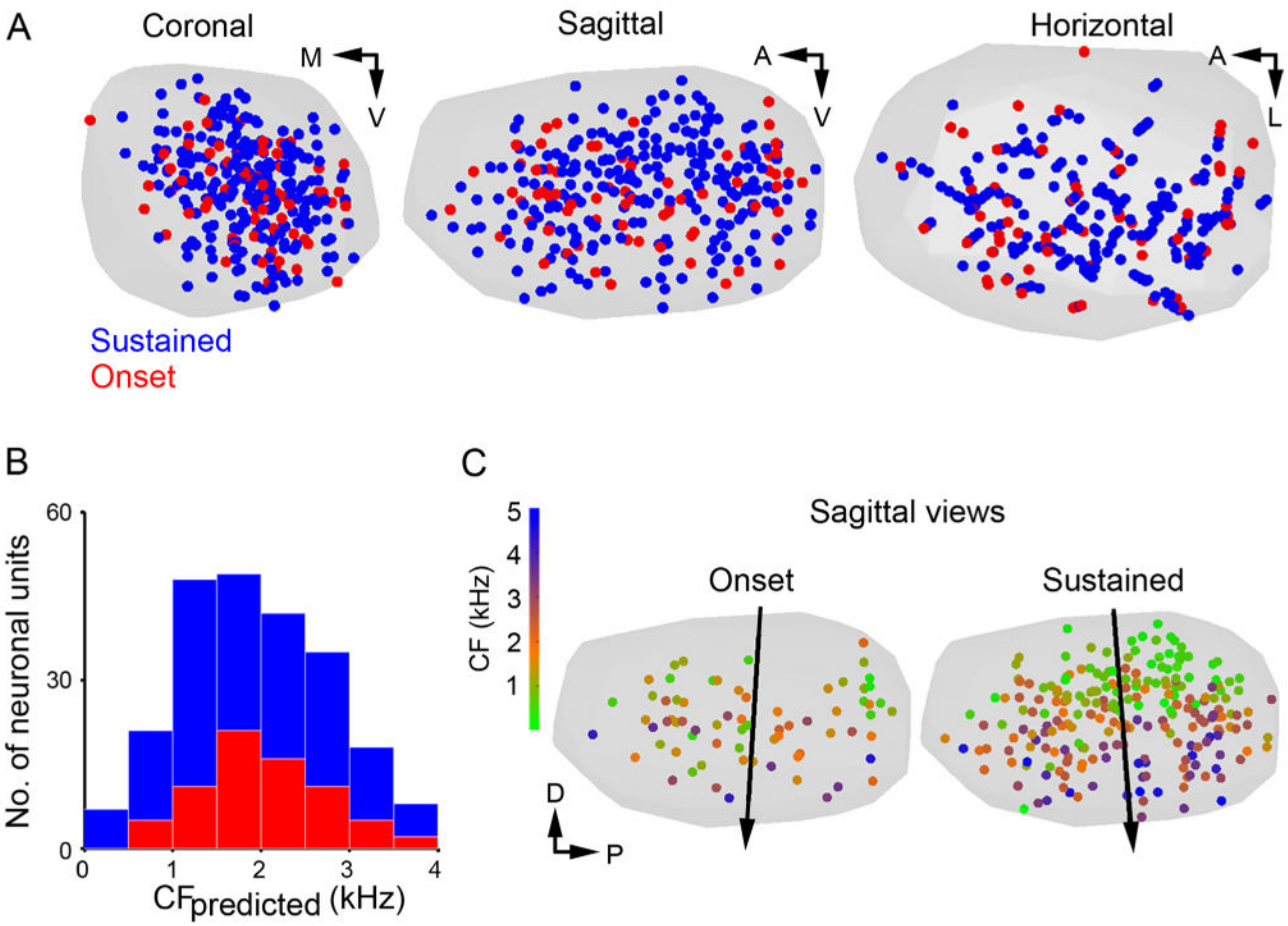

Figure 8.

Sustained and onset responders are interspersed throughout the SON. **A:** Coronal (left), sagittal (center), and horizontal (right) views of a standardized SON (gray hull). Locations of sustained (blue circles) and onset response patterns (red circles) for isolated neuron recordings are shown. No differences were observed in the distribution pattern of sustained and onset responders. **B:** Histograms of predicted CF of sustained (blue) and onset (red) responders confirm broad and similar distributions for each type across the tonotopic axis. **C:** Sagittal views of standardized SON (gray) showing locations of neurons with onset (left) and sustained (right) responses color-coded by CF. See color scale at left. Black arrow indicates orientation of tonotopic axes determined by MRA. Both sustained and onset responders share a dorsal (low CF) to ventral (high CF) tonotopic distribution. Abbreviations: CF, characteristic frequency; A, anterior; D, dorsal; L, lateral; M, medial; P, posterior; V, ventral.

Table 1

Individual Superior Olivary Nucleus (SON) Reconstructions and Standardized SON Show Tonotopic Organization[1]

Case	No. of recording sites	CF mean ± SD (Hz)	Sampled region of SON	Regression function type	r^2	F value	*P* value	$\Theta_{M\text{-}L}$(degrees)	$\Theta_{A\text{-}P}$(degrees)
100726	21	1,864 ± 800	L	Linear	0.51	5.8	<0.01	−0.8	39.8
100727	55	1,612 ± 975	A, P, and L	Linear	0.51	17.7	<0.001	−19.5	−19.9
100729	24	2,328 ± 869	L	Linear	0.62	10.7	<0.001	−31.5	19.1
100801	59	1,475 ± 944	A, P, and M	Linear	0.6	28.1	<0.001	−42.2	7.7
100803	75	1,992 ± 1,352	A, P, and M	Linear	0.61	36.5	<0.001	−28.6	5.6
100804	25	2,101 ± 1,527	P	Linear	0.81	30.6	<0.001	−5.6	−17.8
100810	12	2,542 ± 1,107	P				>0.05		
100811	51	2,478 ± 1,453	P	Linear	0.85	86.7	<0.001	−0.1	−5.8
100812	67	1,770 ± 1,228	M	Linear	0.58	28.6	<0.001	−4.6	−5.7
100813	28	1,493 ± 860	P	Linear	0.83	39.4	<0.001	−23.8	−8.4
100816	19	1,786 ± 1,008	M and L	Log	0.49	48	<0.05	51	−6.9
100817	29	1,773 ± 1,333	P and L	Linear	0.69	18.1	<0.001	2.3	−49.8
100818	13	2,055 ± 1,207	A	Linear	0.86	18.5	<0.001	83.1	−52.6
110224	32	2,452 ± 1,216	P	Linear	0.67	18	<0.001	−73.7	−39.5
110226	43	1,889 ± 1,102	M	Log	0.67	26.9	<0.001	−30.8	−3.6
110228	21	2,040 ± 1,108	A				>0.05		
110301	24	2,400 ± 1,124	A and L	Linear	0.6	9.9	<0.001	34.2	−28.3
110302	30	1,847 ± 940	P and L	Linear	0.51	8.9	<0.01	19.7	−21
110303	31	2,117 ± 1,018	A	Linear	0.59	7.9	<0.01	17.4	−0.2
Mean ± SD	35 ± 19	1,992 ± 344			0.65 ± 0.13			−4.4 ± 38	−12 ± 24
Combined	659	1,935 ± 1,210	Entire SON	Linear	0.62	182	<0.001	−4.5	−7.7
Onset	80	1,690 ± 1,031	Entire SON	Linear	0.45	8.6	<0.01	−5.9	3.5
Sustained	233	1,870 ± 1,214	Entire SON	Linear	0.64	68.3	<0.001	−2.7	−4.4

[1]Statistics presented for the regression function (linear or log) with the greatest r^2 value. Positive $\Theta_{M\text{-}L}$ values indicate tonotopic axes oriented from dorsolateral to ventromedial compared with dorsal-ventral axis. Positive $\Theta_{A\text{-}P}$ values indicate tonotopic axes oriented from dorsoposterior to ventroanterior compared with dorsal-ventral axis. F value used to test significance of the MRA. Abbreviations: A, anterior; L, lateral; M, medial; P, posterior.